Dynamic Properties of Thermoplastic Butadiene–Styrene (SBS) and Oxidized Short Carbon Fiber Composite Materials

LUIS IBARRA, DAVID PAÑOS

Instituto de Ciencia y Tecnología de Polímeros (C.S.I.C.), c/Juan de la Cierva, 3, 28006 Madrid, Spain

Received 3 February 1997; accepted 15 May 1997

ABSTRACT: In composites consisting of a thermoplastic butadiene–styrene (SBS) elastomer matrix reinforced with oxidized short carbon fiber, scanning electron microscopy (SEM) reveals the existence of matrix–fiber interactions, which are not detected when employing commercial carbon fiber. Interpretation of the dynamic properties and other parameters, such as equivalent interfacial thickness, and glass transition temperature, measured in terms of maximum damping temperature, as well as the apparent activation energy of the relaxation process, helps to explain the existence of such interactions.
© 1998 John Wiley & Sons, Inc. J Appl Polym Sci **67:** 1819–1826, 1998

Key words: composites; elastomeric matrix; carbon fibers; dynamic properties

INTRODUCTION

When property improvement of composite materials is at stake, it is essential to promote matrix–fiber adhesion, which ensures effective stress transfer. Elastomeric matrix and short fiber composites combine the stiffness and strength of the fiber with the elasticity and flexibility of the matrix, which explains the growing number of research efforts devoted to these materials, which, apart from these two characteristics, highlight the importance of other factors, such as fiber orientation in the matrix (originating property anisotropy), fiber dispersion, and the postprocessing length to diameter ratio.

The high shear stresses required in elastomer processing for adequate filler dispersion have a considerable effect on the final length to diameter (L/d) ratio in such a way that, in many cases, the beneficial effect of the filler is cancelled out. This is the reason why glass and carbon fibers are not the most appropriate fillers for the type of matrix under discussion. Fortunately, thermoplastic elastomer processing requires lower shear stresses, which means lesser fiber deterioration.

The main problem, however, is and remains the achievement of strong fiber–matrix adhesion, a field that has attracted a lot of major research efforts. In our laboratory, these efforts were aimed in the following three directions: addition of conventional adhesive systems, of the resin phenol–formaldehyde type[1]; fiber surface modification with reagents capable of subsequent reaction with the polymeric chain, i.e., with azide derivatives[2,3]; and, finally, increase of surface functionality, in particular that of carbon fiber,[4] with consistently satisfactory results.

As regards carbon fibers, their low surface energy makes them unable to create strong links with the matrix.[5] Nevertheless, the possibility of increasing this energy by means of surface treatments, mainly of the oxidative type,[6] opens up new perspectives in the field of composite materials.

In this work, the dynamic properties are measured in composites consisting of a thermoplastic

Correspondence: L. Ibarra. E-mail: ICTIR00@FRESNO.CSIC.ES

Journal of Applied Polymer Science, Vol. 67, 1819–1826 (1998)
© 1998 John Wiley & Sons, Inc. CCC 0021-8995/98/101819-08

Table I Fiber Characteristics

Fiber Type	Specific Surface Area (m^2/g)	μ Equivalent (COOH/g)	Fiber Strength (MPa)	Aspect Ratio (L/d)
Commercial	0.48	28.5	2962	744
Oxidized A	0.66	110.5	2343	930
Oxidized B	0.66	191	623	564

butadiene–styrene elastomer matrix (SBS) reinforced with carbon fiber subjected to oxidative treatment to enhance surface functionality and, hence, surface energy, at variable strain amplitude, temperature, and frequency. The dynamic properties are interpreted in terms of the interface formed, as determined by scanning electron microscopy (SEM).

EXPERIMENTAL

Materials and Composite Preparation

The elastomeric matrix was a butadiene-styrene (SBS) copolymer block with a radial structure, polymerized in solution, and supplied by Repsol Química S.A. under the trade name Calprene 416.

A cylindrical polyacrylonitrile (PAN) carbon fiber of approximately 5 μm diameter was used, supplied by Hercules Aerospace España S.A. under the trade name 1815/AS. Fiber oxidation was described in a previous work,[7] varying the treatment time in order to obtain different levels of oxidation. The characteristics of the oxidized fibers used are compiled in Table I, together with those referring to the untreated commercial fiber. The mean fiber lengths and aspect (length to diameter ratio, L/d) ratios in that table refer to postprocessing measurements.

For each of the fiber types obtained at different treatment times, composites were prepared containing a fiber portion of 12 parts in weight per 100 of polymer. All the blends were prepared under the same conditions, as follows: the components were blended in a two-roll mill [friction ratio (speed differential between them) was 1 : 1.25; length was 300 mm], heated by a thermofluid to a temperature of 140 $\pm$ 5°C, and the same flow direction was maintained in order to favor uniform fiber orientation within the matrix. Finally, the samples were rolled to 2 mm thick slabs.

The samples were molded in a thermofluid-heated compression press at 190°C, holding them at that temperature for 15 min. Then the die was placed on a cold plate, applying pressure for 5 min.

Scanning Electron Microscopy

The SEM photographs were taken with a JEOL microscope, Model T330A, at the ruptured face of the tensile test samples after testing.

Dynamic Properties

The viscoelastic properties of the composites were measured in a Metravib viscoanalyzer RAC 815A, set at variable strain amplitude, temperature, and frequency conditions. The sample used was a parallelepiped, with approximate dimensions of 15 $\times$ 6 $\times$ 2 mm.

The properties were measured in three directions, in relation to preferential fiber orientation: longitudinal (L), transversal (T), and forming a 45° angle. Sample preparation allowing for strain application in these three directions to preferential fiber orientation did not pose any problem at all. It was sufficient to cut the samples from the slab at 0, 45, and 90° angles to the flow direction of the blend.

RESULTS AND DISCUSSION

Scanning Electron Microscopy

Figures 1–5 show the different SEM photographs of the ruptured surface in the tensile-tested samples. The surface of the sample containing commercial fiber is shown to be clean and free of any adhesions or links to the polymeric matrix (Figs. 1 and 2). In contrast, in the materials filled with oxidized fiber (Figs. 3–5), the elongation broken surface presents a matrix linked to the fiber surface. These photographs are sufficient and unequivocal evidence of the existence of matrix–fiber links, which condition the properties of the end

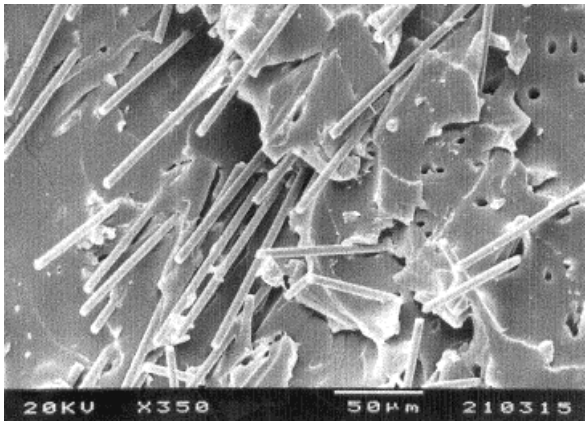

Figure 1 SEM photography of composite reinforced with commercial fiber (350×).

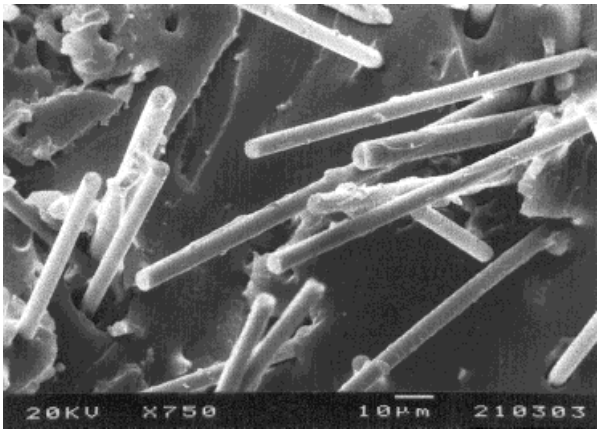

Figure 3 SEM photography of composite reinforced with oxidized type A fiber (750×).

product, as was stated, regarding the mechanical properties and the stress–strain behavior.[8]

Dynamic Properties at Variable Strain Amplitude

Figure 6 shows storage modulus E' variation as a function of strain amplitude, in terms of double strain amplitude (DSA, %), for the different composites, and taking into account the angle formed by the deviation of preferential fiber orientation to the direction of stress application, i.e., 0° (longitudinal to fiber orientation), 45°, or 90° (transversal).

For all composites, the graphs follow the same trend, with more or less marked variations, depending on fiber type and the strain incidence angle used. Low strain causes a first zone of slight modulus variation, which, in some cases, is practically horizontal, thus pointing towards a linear response zone. It is followed, as of a certain strain amplitude, by a second zone of more or less drastic modulus drop.

By the same token, for all graphs, a marked anisotropy is observed, where the modulus decreases with increasing strain incidence angle. This phenomenon can be explained by the fact that, at a 0° angle, i.e., longitudinal strain application, a matrix–fiber deformation as a whole is produced; hence, the modulus value is more strongly affected by fiber stiffness. With increasing orientation angle, strain has a stronger, even exclusive (90° angle) incidence on the matrix so that the lowest modulus values correspond to strain application transversally to fiber orientation.

Furthermore, for one and the same strain incidence angle, the storage modulus values are

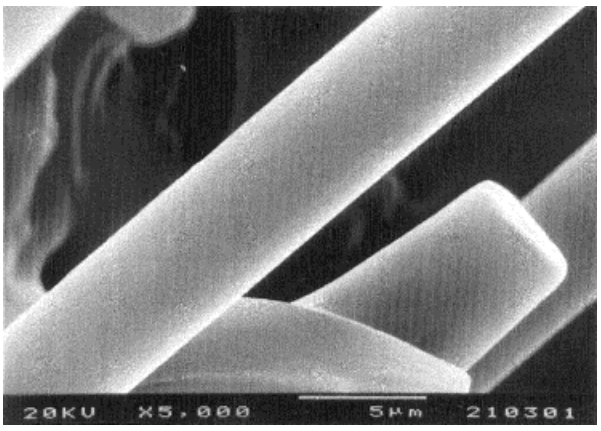

Figure 2 SEM photography of composite reinforced with commercial fiber (5000×).

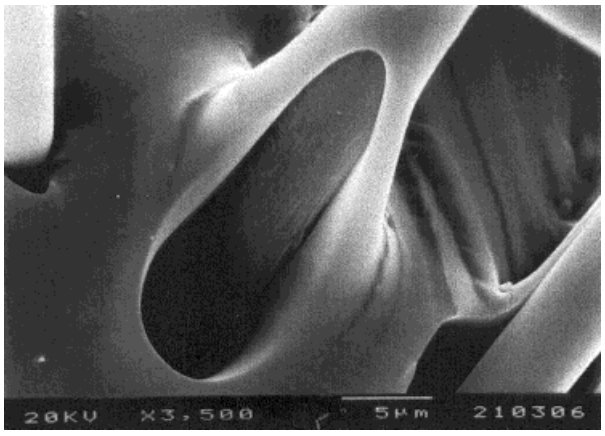

Figure 4 SEM photography of composite reinforced with oxidized type A fiber, 3500×.

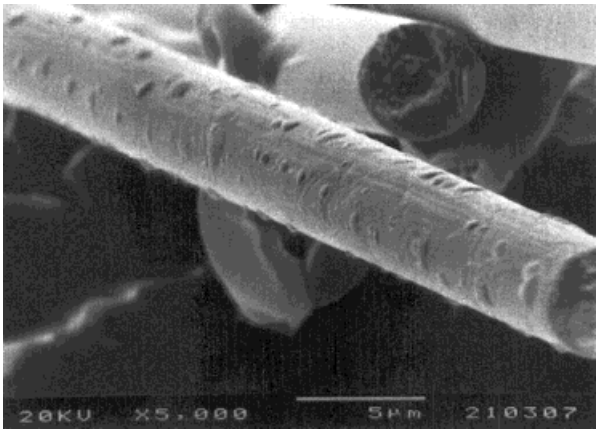

Figure 5 SEM photography of composite reinforced with oxidized type B fiber, 5000×.

higher for the samples containing oxidized fiber but diminish as the oxidation level increases.

In the composites, the initial modulus value is the one resulting from the sum of factors, such as matrix and fiber types, fiber portion, stiffness of one and the other phase, and the number of existing matrix–fiber links. It could be expected, in principle, that for a certain angle, all materials should yield the same modulus value. So the differences observed experimentally can only be explained in terms of fiber treatment and the existence of matrix–fiber links.

The matrix–fiber links, as evidenced by SEM, explain the high modulus values in the samples filled with oxidized fiber, whereas the modulus drop for the sample containing fiber with the highest degree of oxidation (type B) has to be explained in terms of a smaller L/d ratio in these fibers, as a consequence of prolonged treatment time, hence, translating into a loss in strength (Table I).[9]

The effect of the increase in strain amplitude on the drop of the storage modulus has been widely studied in particle-filled matrices,[10] with the drop being attributed to the rupture of matrix–filler links. By analogy, in this case, the modulus decrease is to be attributed also to matrix–fiber link rupture.

The higher oxidation grade gives rise to more intense fiber functionalization and hence to a greater number of matrix–fiber links, which, in turn, translate into a lesser modulus drop. Table II shows the E' values for two extreme strains, 0.02 and 4% DSA, the last column indicating the modulus retention percentage, which proves to be greater for materials containing fiber of higher oxidation grades (type B).

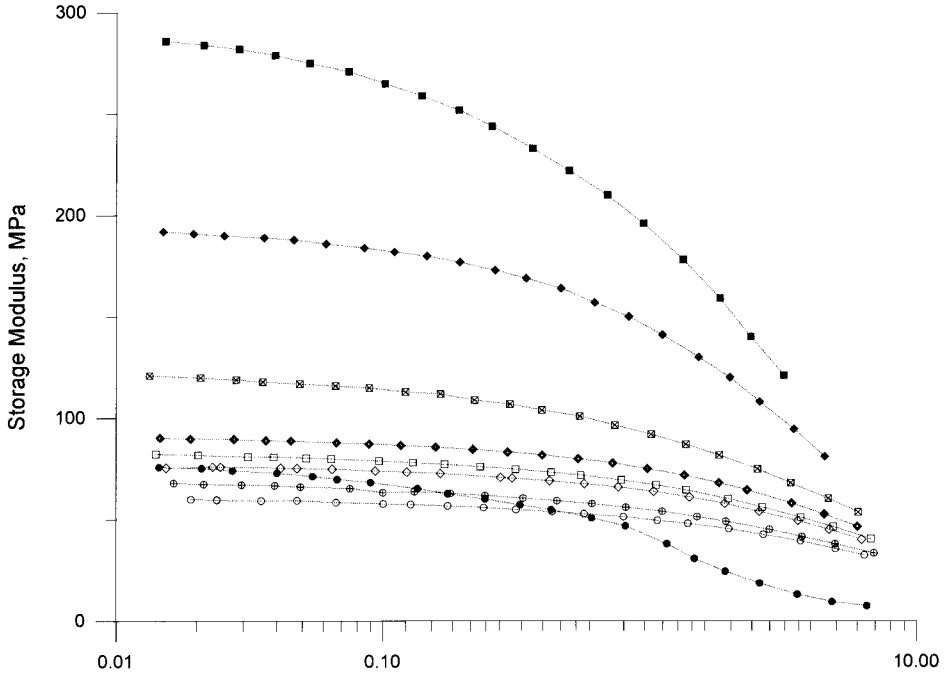

Figure 6 Storage modulus E' as a function of double strain amplitude at three orientation angles (0, 45, and 90°) in composites reinforced with (●, ⊕, ○) commercial fiber, (■, ⊠, □) oxidized type A fiber, and (◆, ◇, ◇) oxidized type B fiber.

Table II Modulus E' Retention in Composites

Fiber Type	Modulus E' (MPa) 0.02% DSA	4% DSA	% Retention
Commercial	75.1	11.8	15.7
Oxidized A	283.5	103.5	36.5
Oxidized B	190.4	87.2	45.8

Conditions are as follows: longitudinal direction; room temperature; 15 Hz vibration frequency.

Figure 7 shows the variations of the loss factor, tan δ, plotted against strain amplitude. The loss tangent varies notably as a function of fiber treatment. Thus, the composite filled with commercial fiber presents an important tan δ increase with increasing amplitude. In this latter case, the interfacial region is weak and does not resist major strain without breakage,[11] which proves the tan δ increment to be associated to matrix–filler friction phenomena. In contrast, whenever there exists a strong interface, the material resists high strain, and the loss factor does not show such increment. The lower values in the material containing oxidized fiber with the longest treatment time are indicative of the existence of a greater number of interactions, as corresponds to a higher degree of fiber functionalization.

The effect of the interfacial region on the dynamic properties can be quantified fairly accurately. By way of a first approximation, the assumption is made that the mechanical loss factor tan δ of the composite (tan δ_c) can be expressed as follows[12,13]:

$$\tan \delta_c = V_f \tan \delta_f + V_i \tan \delta_i + V_m \tan \delta_m, \quad (1)$$

where the subscripts f, i, and m refer to the filler, the interface, and the matrix, respectively, and V is the respective volume fraction. This equation does not supply a detailed prediction of the loss factor of the composite, as it involves a combination of serial and parallel phase couplings; yet it is useful as a starting point, when the effect of different surface treatments on interfacial adhesion is to be compared. Assuming that tan $\delta_f = 0$ and that the interfacial volume fraction V_i is very small, eq. (1) can be rewritten as follows:

$$\tan \delta_c / \tan \delta_m = (1 - V_f)(1 + A), \quad (2)$$

where

$$A = \frac{V_i}{1 - V_f} * \frac{\tan \delta_i}{\tan \delta_m} \quad (3)$$

Hence, factor A can be defined as a function of known or determinable value:

$$A = \frac{1}{1 - V_f} * \frac{\tan \delta_c}{\tan \delta_m} - 1 \quad (4)$$

The strong interactions between the filler and the matrix at the interface tend to reduce macromolecular mobility in the fiber surface environment, as compared to mobility at other regions in the matrix. This fact also reduces tan δ_i and hence A; a low A value is indicative of a high degree of fiber-matrix interaction or adhesion at the interface.[14]

Y. H. Zhou introduces a new concept, that of equivalent interfacial thickness, R[15], as derived from the Halpin–Tsai equation.[16] This concept substantiates the idea that the interface can be understood as a uniform layer, assuming that property variation in short fiber-reinforced materials generated at the interface is a consequence of an increment in fiber radius in such a way that greater ΔR will stand for stronger interfacial action.

ΔR is expressed as

$$\Delta R = R_O(\sqrt{B - 1}) \quad (5)$$

where R_O is the fiber radius, and B can be determined by means of

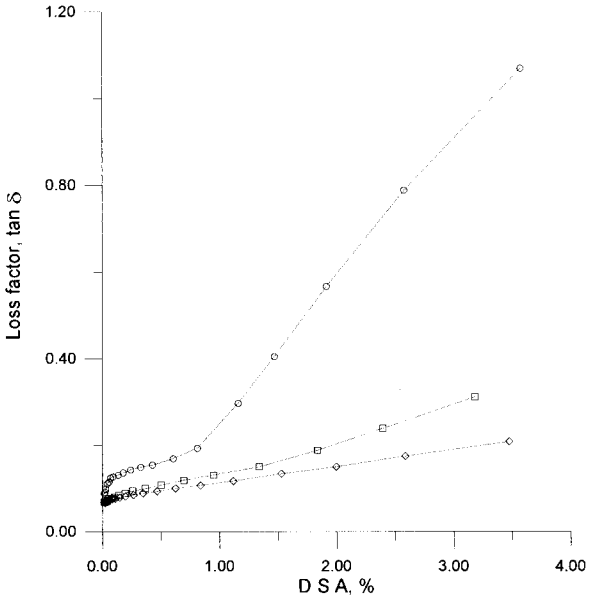

Figure 7 Loss factor, tan δ, as a function of DSA in composite reinforced with (○) commercial fiber, (□) oxidized type A fiber, and (◇) oxidized type B fiber.

Table III Parameter A and Equivalent Interfacial Thickness ΔR Values as a Function of DSA in Composites

DSA (%)	Parameter	Commercial Fiber	Oxidized A Fiber	Oxidized B Fiber
0.1	A	0.79	0.12	0.065
0.1	ΔR	4.74	5.84	5.63
1	A	2.45	0.79	0.55
1	ΔR	4.19	5.38	5.20
3	A	11.21	2.99	1.56
3	ΔR	3.49	4.69	4.52

$$\frac{(E'_T/E'_M) - 1}{(E'_T/E'_M) + 2} = B * V_f \qquad (6)$$

where E'_T is the storage modulus of the composite, measured transversally; E'_M is that of the matrix; and V_f is the fiber volume fraction.

Table III compares the values of A and R parameters calculated at different double strain amplitude (DSA), which are indicative of the existence of a high degree of phase interactions in oxidized fiber-reinforced composite.

Dynamic Properties at Variable Temperature and Frequency

When dynamic properties, in particular, loss factor tan δ, are determined as a function of temperature at a given frequency, the relaxation spectrum of the material is obtained, which presents the major relaxation episodes in the form of peaks. Figure 8 shows the variation of tan δ of the composites as a function of temperature, applying sine wave strain longitudinally to preferential fiber orientation.

The spectra present two peaks: the first one corresponds to the glass transition of the butadiene blocks in the matrix, at low temperature; the other one, at high temperature range, indicates the softening of the stiff styrene blocks. Although there is overlap of the zones in which the two damping peaks appear, the temperatures at which they present are divergent, with their range defining the glass transition of the composite.

Table IV lists the values of the damping peak temperatures, corresponding to the glass transition of the material, together with the tan δ values at the different experimental frequencies, with the stress being applied longitudinal and transversal to preferential fiber orientation. The values of damping peak temperatures have been calculated by fitting the experimental points to a polynomial equation.

The glass transition temperature of the material is influenced by the existence of matrix–filler interactions, in such a way that whenever they exist, they will cause the glass transition point to shift towards higher temperature ranges. The values listed in the table show that, upon oxidized fiber incorporation into the material, the damping peak also rises as a function of oxidation grade, as compared to the commercial fiber composite. The greatest differences are recorded for longitudinally applied strain. Likewise, temperature also rises with increasing vibration frequency.

These temperature shifts with frequency increase allow calculation of an apparent activation energy of the relaxation process, ΔE, by means of the following equation[17]:

$$\log f = \log f_O + E/2{,}303\, RT, \qquad (7)$$

where f is the vibration frequency, and T the absolute temperature at the maximum damping peak at frequency f.

The ΔE values are given in the last line of Table IV. They are independent of fiber orientation but always higher in the oxidized fiber samples, with the higher values owing to the existence of matrix–fiber interactions.

Maximum damping peak amplitude and tan δ at glass transition temperature diminish in the samples containing treated fiber in comparison with the commercial fiber material, with the greatest differences being recorded for longitudinal strain. According to other authors,[18] the maximum value of tan δ, measured transversally, and for the principal matrix relaxation decreases linearly with increasing fiber volume fraction V_f, with the intercept at the ordinate coinciding with the value of tan δ of the unfilled matrix. As a consequence, the value of tan $\delta\perp_{\max}$ in the composite can be expressed as

$$(\tan \delta\perp_{\max})_C = (\tan \delta_{\max})_M - \alpha V_f, \qquad (8)$$

representing α, a fiber-type dependent coefficient, from whose value the degree of fiber-matrix interaction can be estimated in such a way that the further it moves away from the unit, the higher the degree of interaction. Table V compiles the

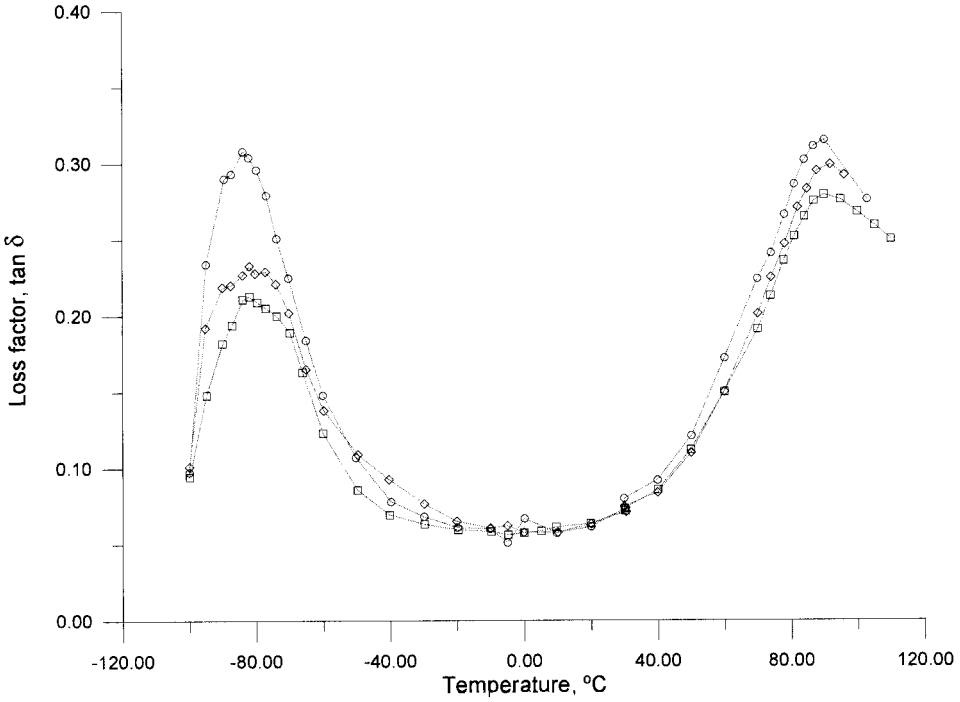

Figure 8 Loss factor, tan δ, as a function of temperature in composites with (○) commercial fiber, (□) oxidized type A fiber, and (◇) oxidized type B fiber. Strain amplitude: DSA = 0.013%.

values calculated for α at each frequency, together with the values used for $\tan(\delta_{max})_M$, assuming $V_f = 0.0615$.

At any frequency, the value of α calculated for the material containing oxidized type A fiber is considerably higher, indicating a high degree of interaction. The lower values obtained for the type B fiber samples are attributable to a lower

Table IV Maximum Damping Temperatures and Amplitude at Different Frequencies

	Commercial		Oxidized A		Oxidized B	
Frequency (Hz)	T (°C)	tan (δ_{max})	T (°C)	tan (δ_{max})	T (°C)	tan (δ_{max})
			Longitudinal Direction			
5	−84.95	0.309	−80.07	0.212	−78.98	0.230
7, 9	−83.89	0.314	−77.27	0.218	−78.59	0.235
12, 6	−82.37	0.323	−76.27	0.230	−77.18	0.243
20	−80.68	0.333	−75.73	0.240	−75.21	0.250
ΔE (kJ mol)	103.3		132.9		133.0	
			Transversal Direction			
5	−84.13	0.350	−82.32	0.256	−82.05	0.339
7, 9	−82.66	0.353	−82.05	0.261	−81.15	0.340
12, 6	−81.25	0.361	−80.26	0.271	−80.11	0.348
20	−80.00	0.370	−78.26	0.279	−78.69	0.358
ΔE (kJ mol)	97.0		141.8		133.0	

Table V α Values at Different Frequencies

Fiber Type	5 Hz	8 Hz	12, 5 Hz	20 Hz
tan $(\delta_{max})_m$	0.471	0.481	0.494	0.496
Commercial	4.16	4.33	4.36	4.14
Oxidized A	7.41	7.41	7.32	7.10
Oxidized B	4.55	4.74	4.80	4.53

L/d ratio, which counteracts the proven matrix–fiber interactions.

CONCLUSIONS

In the light of our discussion, the following conclusions may be arrived.

1. Oxidative treatment increases the surface functionality of carbon fiber, in terms of acidity, and promotes bonding with the matrix, which does not occur with untreated commercial fiber, as demonstrated by SEM.
2. The existence of matrix–fiber interactions conditions the dynamic properties of the materials. The composites present significantly higher storage moduli at any strain amplitude and independent of the strain application angle, although the differences decrease with increasing strain angle.
3. As fiber treatment is prolonged, a loss in fiber strength takes place, derived from the reduced L/d ratio, which translates into lower modulus values. Nevertheless, modulus retention at greater strain amplitudes is higher, as a consequence of the greater number of matrix–fiber.
4. The oxidized fiber composites possess lower tan δ values due to the fact that the links between the phases are able to resist considerable strain without breaking, thus also avoiding the friction phenomena, which cause tan δ to increase.
5. The increments in equivalent interfacial thickness, the glass transition temperature of the material, and the apparent activation energy of the relaxation process, together with the variations observed for other parameters, factor A and α-coefficient, jointly supply evidence of the existence of matrix–fiber interactions in the composites filled with treated fiber.

The authors thank to CICYT for financial support of this work through his Project MAT 95/0099.

REFERENCES

1. L. Ibarra and C. Chamorro, *J. Appl. Polym. Sci.,* **43,** 1805 (1991).
2. M. Arroyo, M. Tejera, and L. Ibarra, *J. Appl. Polym. Sci.,* **48,** 1009 (1993).
3. L. Ibarra and C. Jordá, *J. Appl. Polym. Sci.,* **48,** 375 (1993).
4. L. Ibarra, A. Macias, and E. Palma, *Kauts. Gummi Kunstst.,* **48,** 180 (1995).
5. B. S. Jin, B. S. Lee, and C. R. Choe, *Polym. Inter.,* **34,** 181 (1994).
6. J. B. Donnet and R. C. Bausal, *Carbon Fibers,* Marcel Dekker, New York, 1990, Chap. 3, p. 145.
7. E. Palma and L. Ibarra, *Angew. Makromol. Chem.,* **202,** 111 (1994).
8. L. Ibarra and D. Paños, *Polym. Inter.,* **43,** 251 (1997).
9. G. Dagli and N. H. Sung, *Polym. Compos.,* **10,** 109 (1989).
10. A. I. Medalia, *Rubber Chem. Technol.,* **51**(3), 437 (1978).
11. J. D. Miller, H. Ishida, and F. H. Maurer, *Polym. Compos.,* **9,** 12 (1988).
12. L. E. Nielsen, *Mechanical Properties of Polymers and Composites,* Vol. 2, Dekker, New York, 1974.
13. P. S. Chua, *Polym. Compos.,* **8,** 308 (1987).
14. J. Kubat, M. Rigdahl, and M. Welander, *J. Appl. Polym. Sci.,* **39,** 1527 (1990).
15. Y. H. Zhou, T. Chen, W. D. Wu, C. Li, D. H. Li, and L. Q. Zhang, *Macromolecular Reports,* **A30** (Suppl. 5), 365 (1993).
16. D. Short, *Fibre Composite Hybrid Materials,* MacMillan Publishing Company, New York, 1981, Chap. 3, p. 69.
17. M. Ashida, T. Noguchi, and S. Mashimo, *J. Appl. Polym. Sci.,* **30,** 1011 (1985).
18. M. Ashida, T. Noguchi, and S. Mashimo, *J. Appl. Polym. Sci.,* **29,** 661 (1984).